Investigation of the links between water vapor field evolution and rain rate based on 5 years of measurements at a midlatitude site

Laurent Labbouz, Joël van Baelen, Christophe Duroure

AGU PUBLICATIONS

Geophysical Research Letters

RESEARCH LETTER
10.1002/2015GL066048

Key Points:
- IWV maximum occurs on average 20 min before rain maximum
- In 76% of the cases the IWV peak occurs before the rain peak
- First steps toward building an IWV-based indicator for precipitation nowcasting

Supporting Information:
- Text S1 and Figures S1–S3

Correspondence to:
L. Labbouz,
Laurent.Labbouz@physics.ox.ac.uk

Citation:
Labbouz, L., J. Van Baelen, and C. Duroure (2015), Investigation of the links between water vapor field evolution and rain rate based on 5 years of measurements at a midlatitude site, *Geophys. Res. Lett.*, *42*, 9538–9545, doi:10.1002/2015GL066048.

Received 3 SEP 2015
Accepted 20 OCT 2015
Accepted article online 26 OCT 2015
Published online 11 NOV 2015

Investigation of the links between water vapor field evolution and rain rate based on 5 years of measurements at a midlatitude site

Laurent Labbouz[1,2], Joël Van Baelen[1], and Christophe Duroure[1]

[1]Laboratoire de Météorologie Physique, UMR 6016, CNRS and Université Blaise Pascal, Clermont-Ferrand, France, [2]Now at Department of Physics, University of Oxford, Oxford, UK

Abstract Based on 5 years of measurements of integrated water vapor (IWV), surface mixing ratio (MR), and rain rate, we investigate the relationship between the water vapor field evolution and the precipitation lifecycle. We show that in 76% of the cases the IWV reaches a maximum before the peak of precipitation, with the precipitation peak occurring on average 20 min after the IWV maximum. This delay can be related to the fall time of the precipitation. We also show that the moister the atmosphere, the greater the precipitation rates and the longer the delay. Unlike the IWV, the MR reaches a maximum after the precipitation peak in 60% of the cases, highlighting the interest of IWV compared to surface MR only. This paper and the discussions within it open a pathway to complementary studies and applications for heavy precipitation prediction.

1. Introduction

The role of water vapor convergence and accumulation for the initiation of precipitation has been shown and discussed in numerous studies [e.g., *Trenberth et al.*, 2003; *Kalthoff et al.*, 2009; *Sherwood et al.*, 2010], while accurate knowledge of the water vapor field is needed to produce high-quality precipitation forecasts within a short time frame [*Ducrocq et al.*, 2002]. Nowadays, the amount of integrated water vapor (IWV) from the surface to the top of the atmosphere can be measured from a Global Positioning System (GPS) receiver [*Bevis et al.*, 1992] with good accuracy for ground-based [*Tregoning et al.*, 1998; *Van Baelen et al.*, 2005; *Bonafoni et al.*, 2013] and ocean-based measurements [*Kealy et al.*, 2012]. The GPS measurements can be performed continuously, at a high temporal resolution and under all weather conditions, with condensed water (precipitation and clouds) having only negligible impact on the GPS-based IWV retrievals [*Solheim et al.*, 1999]. The GPS-derived IWV is therefore sensitive only to the water vapor field and with everything else held constant any condensation of vapor will lead to the expected decrease in the GPS-IWV. Water vapor retrievals obtained from GPS have proved to be useful for case studies of precipitation formation and water vapor field evolution [*Champollion et al.*, 2004, 2009; *Bastin et al.*, 2005; *Sato and Kimura*, 2005; *Van Baelen et al.*, 2011; *Manning et al.*, 2012; *Labbouz et al.*, 2013; *Planche et al.*, 2013; *Weckwerth et al.*, 2014].

In this context, the aim of this paper is to investigate the links between the temporal evolution of IWV and the formation of precipitation, based on 5 years of collocated GPS and rain gauge measurements. From 2 months of measurements, *Brenot et al.* [2014] have shown that high IWV values are usually associated with precipitation. Several other studies have shown similar results and have tried to analyze the relationship between IWV evolution and precipitation formation [e.g., *Champollion et al.*, 2004, 2009; *Van Baelen and Penide*, 2009; *Van Baelen et al.*, 2011]. Longer-term microwave radiometer (MWR) measurements from a tropical island have shown that high IWV tends to be measured an hour after the peak of precipitation [*Holloway and Neelin*, 2010]. However, they also showed that high IWV is associated with increased probability of precipitation for the following 10–12 hours and conceded that they cannot claim that their results are applicable to any area other than the tropical ocean.

Our study, based on the use of a GPS receiver for the measurement of IWV, allowed for continuous measurement during heavy precipitation events (which is not usually the case using an MWR, as mentioned by *Holloway and Neelin* [2010]). This allows us to provide a detailed analysis of the links between the water vapor field and the formation of precipitation, over medium to short (5 min) time scales, at a midlatitude continental site. Our analysis is based on a simple statistical method, inspired from the ideas developed by *Mazany et al.* [2002], who combined IWV temporal evolution from GPS measurement with other data in order to build

an index for short-term lightning prediction. For their analysis they used lightning discharges as a temporal reference and studied the evolution of IWV before the first lightning stroke. Here we follow a similar approach using rain rate peaks as a temporal reference.

Building an index as done by *Mazany et al.* [2002] but for local precipitation prediction would be very challenging knowing the complexity and the variety of precipitation processes. Nonetheless, this paper can be considered as a first step in that direction, as we investigate the relative timing of the IWV maximum with respect to precipitation. Moreover, we aim to open a new pathway for further studies of water vapor-precipitation interaction processes.

In section 2 we present the instruments and the data processing technique as well as the methodology applied. Section 3 focuses on the presentation and discussion of the results. Finally, section 4 provides a summary and outlines the perspectives opened by the current study.

2. Methodology

The data used in this study come from a rain gauge, a GPS receiver, and meteorological probes for pressure, temperature, and water vapor mixing ratio (MR hereafter) located on the roof of the Laboratoire de Météorologie Physique, in Aubière, France (3.111°E, 45.761°N). The tipping-bucket rain gauge has a resolution of 0.2 mm of accumulated rain and data is recorded every 5 min. The GPS receiver is part of the two permanent French GPS networks: RGP (Réseau GNSS Permanent) and RENAG (Reseau National GPS permanent), and the data have been processed by the Institut national de l'information géographique et forestière (IGN). The zenith total delay (ZTD) is retrieved every 15 min and then the corresponding IWV is calculated using the pressure and temperature measured alongside the GPS antenna:

$$\mathrm{IWV} = [\mathrm{ZTD}–\mathrm{ZHD}]/Q(T)$$

with ZHD the zenith hydrostatic delay, obtained from the pressure, geoidal height and latitude of the antenna [*Saastamoinen*, 1972a, 1972b; *Davis et al.*, 1985], and $Q(T)$ an empirical term derived by *Emardson and Derks* [2000] for central Europe, which depends only on the temperature at the GPS station. The IWV obtained are then linearly interpolated on a 5 min time scale. The data used in the following analysis correspond to the period 30 January 2007 to 29 January 2012.

In order to investigate IWV evolution with respect to precipitation events, we develop a simple method taking the precipitation peaks as temporal references. First, we determine the time t_0 of the heaviest rain rate peak in the 5 years of data considered here. Then we select all the meteorological data in the interval $[t_0 - 9\,\mathrm{h}\,;\, t_0 + 9\,\mathrm{h}]$. The choice of an 18 h interval allows for a description of the prerain and postrain situations and prevents us from considering two events close in time as distinct or considering successive peaks of a single event as separate. Reasonable changes in the interval size have been tested without any significant effect on the results. After excluding the data already selected (i.e., the data within the 18 h interval), we then select the "next" highest rain peak and repeat the procedure. As the detection threshold of the rain gauge is 0.2 mm, in order to avoid "false events," we consider only precipitation peaks with at least 0.4 mm of rain accumulated over 5 min (i.e., more than one bucket oscillation), corresponding to a rain rate of 4.8 mm h^{-1}. Finally, we keep only the N time intervals with more than 90% of available data for all the variables and calculate the sample average G of each meteorological variable g (IWV, MR, and rain rate):

$$G(t) = \sum_{i=1}^{N} \frac{g(t_{0i} + t)}{N}\ ,\ t \in [-9\,h\,;+9\,h]$$

where t_{0i} is the time of the precipitation peak for the interval number i.

3. Results

In this section we focus on the results and their direct implications. More interpretations and discussions are provided in the next section.

3.1. Initial Results

We would like first to highlight the fact that all the analyses made hereafter describe an average behavior, whose sense is also discussed. Over the 5 years of data considered in this study, applying the criteria previously described, we identify 191 precipitation events. We observe that, on average, both IWV and MR increase before

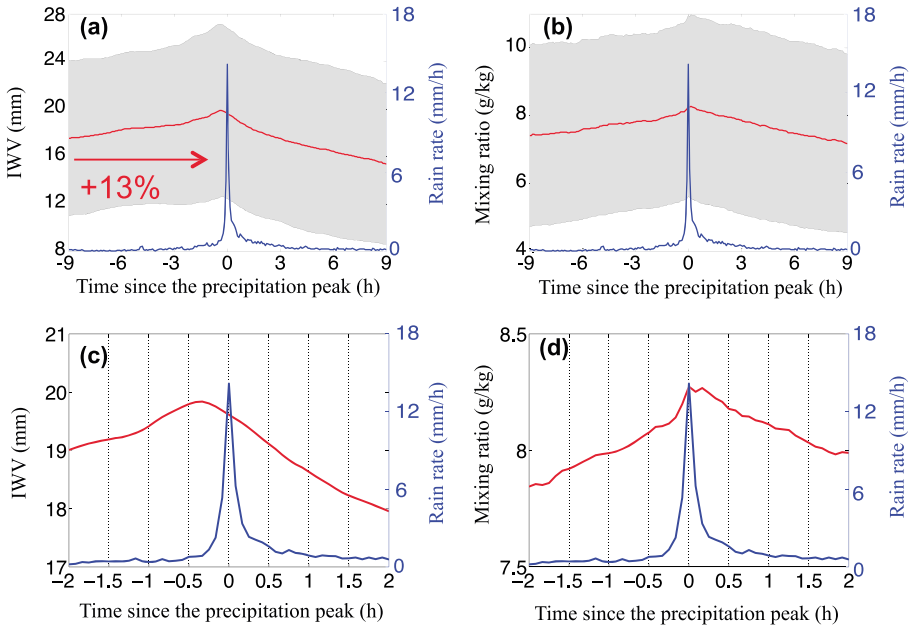

Figure 1. Mean rain rate (blue lines), and mean values of (a and c) IWV and (b and d) mixing ratio (red lines) from 191 rain events with precipitation peak of at least 4.8 mm/h. The grey shading (Figures 1a and 1b) indicates the standard deviation (±1σ). The red arrow and label (Figure 1a) indicate the relative increase of IWV between −9 h and −20 min (maximum of IWV). The bottom plots (Figures 1c and 1d) are zooms of the top graphs (Figures 1a and 1b, respectively).

the onset of precipitation and decrease afterward (Figures 1a and 1b). However, zooming in on the precipitation peak (Figures 1c and 1d) shows that the IWV maximum is reached 20 min before the precipitation peak, whereas the MR maximum occurs at the same time as the precipitation peak and then remains somewhat constant for the following 10 min. Very similar results in terms of the shape and timing of the IWV and MR curves are also observed using another pluviometer located 250 m from the GPS (cf. Figure S1 and Text S1 in the supporting information), far enough away to show that the well-known rain field heterogeneity [e.g., *Ciach*, 2003] does not significantly affect our results but still close enough to be within the GPS-sampled atmosphere.

The results from Figure 1 show that, on average, there is an increase in atmospheric water content before the onset of precipitation. Between −9 h and −20 min, the IWV increases by 13%. The role of moisture accumulation in precipitation formation is well known, but more interesting is the anticipation of the IWV maximum with respect to the rain rate maximum. The results presented in Figure 2 confirm that in most of the cases the IWV maximum is reached before the peak of precipitation. More precisely, 76 % (69%) of the data have their IWV maximum between −5 min and −9 h (−8 h) before the rain rate maximum. The highest numbers of occurrences are found between −15 min and −45 min, corresponding to 23% of the cases. The MR maxima (Figures 2c and 2d) are delayed compared to the IWV maxima (Figures 2a and 2b). In 60% (55%) of the cases, the MR reaches its maximum between +5 min and +9 h (+8 h) after the precipitation peak, with the highest number of occurrences found between 0 and +30 min (22% of the cases). To avoid any arbitrary selection thresholds, Figure 2 does include all the 191 cases considered in this study although some of them do not have a well-defined IWV maximum (e.g., because of a secondary local maximum or because the IWV variation is small).

The differences between MR and IWV observed in both Figure 1 and Figure 2 highlight the importance of IWV measurement from a forecasting perspective. They also indicate that the processes controlling the full troposphere IWV and the surface MR are different, the increase of the MR associated with rain being mostly due to evaporation at the surface. This will be discussed section 4.2.

3.2. Validation and Further Results

The results presented in Figure 1 are the average over 191 different 18 h time intervals, encompassing various meteorological situations encountered over the 5 years of this study. It can be seen that the standard

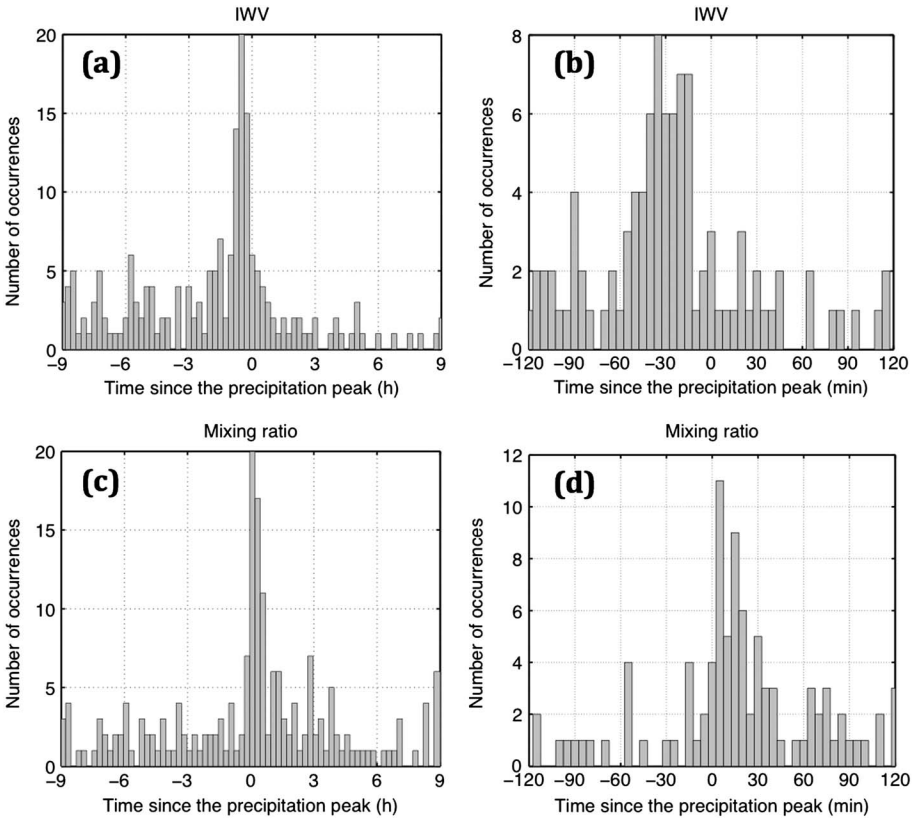

Figure 2. Distributions of the time differences between the peak of precipitation and the maximum of (a and b) IWV and (c and d) mixing ratio for the 191 cases considered in this study. The bin sizes are 15 min (Figures 2a and 2c) and 5 min (Figures 2b and 2d). As mentioned in the text the resolution of the data is 5 min.

deviation is higher than the mean variation observed during the period: the standard deviation approaches 40%, whereas the relative variation of IWV is 13% between the beginning of the period and the maximum. Figure 2a shows that the time distribution of the IWV maximums is highly non-Gaussian, with large tail explaining the high standard deviation. This means that we cannot yet claim our results to be a general conclusion about the links between water vapor and precipitation.

Thus, in order to test the significance of our results, we compare them to those obtained when applying the method described in section 2 to rain-free periods of more than 60 consecutive hours and defining t_{0i} as the time of the middle of that dry period (the corresponding graphs are shown in Figure S2). We observe that the mean variation of IWV and MR associated with precipitation events (Figures 1a and 1b) are much larger than those observed during the dry periods (nearly constant; cf. Text S1 and Figure S2), while variances are quite similar, demonstrating that the observed signal in the mean evolution of IWV and MR associated with precipitation peaks carries a clear physical significance.

To further test the validity of our results and to discriminate between different meteorological conditions, we select different subsets of data based on IWV values. The histogram of the IWV measured 20 min before the precipitation peaks (Figure 3) shows two distinct maxima: one maximum corresponds to medium values of IWV (MIWV cases), between 12.5 mm and 22.5 mm (100 cases, i.e., 52% of the cases), while the other corresponds to high values of IWV (HIWV cases), between 27.5 and 32.5 mm (31 cases, i.e., 16%).

Selecting these two "modes," we apply our analysis method to the respective data subsets to produce the results shown in Figure 4. As expected, we notice that the standard deviation is reduced significantly, whereas the shape of the IWV temporal evolution remains similar to that in Figure 1a. This helps to confirm the validity of our analysis. Furthermore, we also observe that the MIWV cases correspond to lighter rain and to a smaller IWV maximum in absolute value and in relative variation, with an average increase of 11% for the

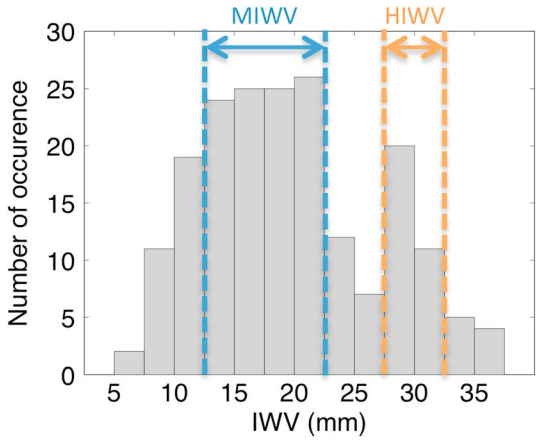

Figure 3. Distribution of the IWV measured 20 min before the peak of precipitation for the 191 cases considered in this study. The medium IWV (MIWV) mode corresponds to IWV between 12.5 and 22.5 mm (100 cases), whereas the high IWV (HIWV) mode corresponds to IWV between 27.5 and 32.5 mm (31 cases).

MIWV cases, compared to 16% in the HIWV cases. Finally, we also observe that the anticipation of the IWV maximum with respect to the precipitation peak is slightly longer in the HIWV case (25 min; cf. Figure S3a for a zoom) than in the MIWV case (15 min; Figure S3b). On the contrary, the MR time evolution in the HIWV cases does not exhibit a clear unique maximum, but instead exhibits nearly constant MR for up to 1.25 h after the precipitation peak (Figure 4b), whereas the MIWV exhibits MR evolution very similar to the one observed on average (Figure 4d compared to Figure 1). The possible implications of these results in term of cloud lifecycle are discussed in the next section.

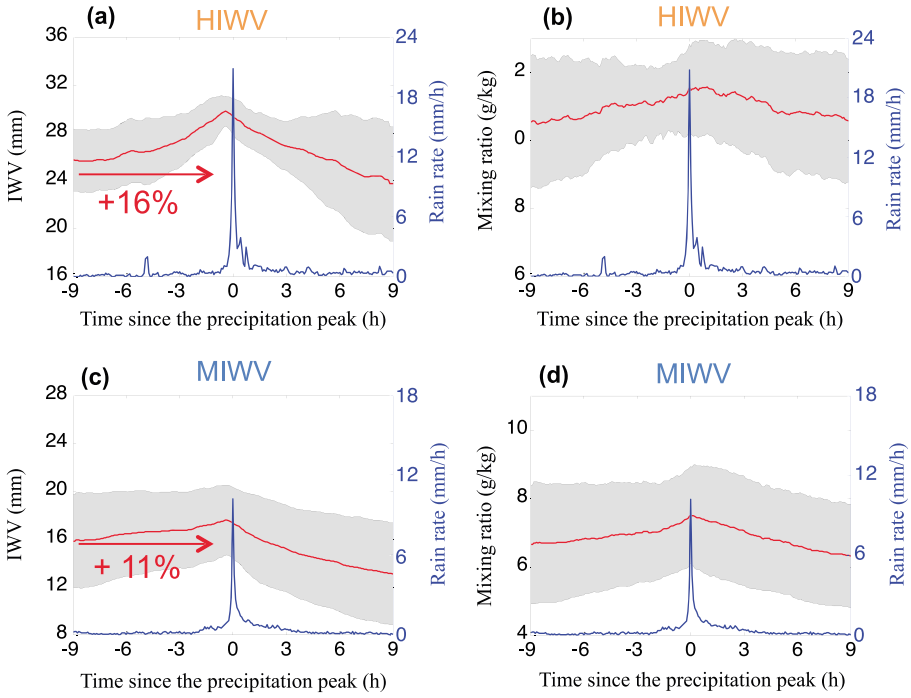

Figure 4. Mean rain rate (blue line), IWV (red line, a and c) and mixing ratio (red line, b and d). The red numbers indicate the relative increase in IWV between −9 h and the maximum of IWV. The top (Figures 4a and 4b) and bottom (Figures 4c and 4d) plots correspond respectively to the MIWV and HIWV data subsets as defined in Figure 3 and in the text. The grey shading shows the standard deviation (±1σ from the mean values).

4. Conclusions and Discussion

4.1. Conclusions

Based on 5 years of collocated meteorological data (mixing ratio and rain rate) at ground level and IWV GPS retrievals in Aubière, France, we provide a simple analysis to investigate the relative timing of IWV and mixing ratio maxima with respect to rainfall maxima.

We show that in the vast majority of cases (76%) the IWV reaches its maximum before the rain rate, while most of the time the mixing ratio at the ground reaches its maximum after the precipitation peak (in 60% of the cases).

A simple method allows us to analyze 191 time series and to show that on average the IWV increases before the onset of precipitation and reaches its maximum 20 min before the peak of precipitation. Both this delay and the relative increase of IWV before the onset of rain are more marked in the cases of high IWV, corresponding to high precipitation rates. The IWV evolution can hence be used as an indicator of precipitation formation, especially in cases of high IWV.

4.2. Discussion

We have seen that on average the IWV increases before the onset of precipitation and decreases afterwards. As a system is forming, we can suppose that there is (on average) a moisture flux convergence, which is the source of water vapor enhancement [cf. e.g., *Banacos and Schultz*, 2005; *Kalthoff et al.*, 2009; *Labbouz et al.*, 2013]. In the case of a convective cloud, the deeper the cloud, the higher the vertically integrated amount of condensate. The cloud development implies water condensation/deposition, and hence is a sink for water vapor, which has to be balanced by increased water vapor convergence in order to sustain the system. Indeed, if the source of water vapor becomes smaller than the condensation sink the entire column will become drier. This is likely to correspond to the most mature stage of the system, as it will start to decay afterward due to lack of incoming humidity.

Hence, the peak of IWV is likely to correspond to the most active part of the system in terms of condensation and subsequent precipitation formation (via autoconversion and accretion), and the observed delay of on average 20 min may be interpreted as the fall time of the precipitation. A droplet with a radius of 2 mm will have a terminal fallspeed of about 5 m s^{-1} [*Beard*, 1976]. Assuming that this was its fallspeed from formation (neglecting the vertical wind and all microphysical processes), the droplet would have fall 6 km in 20 min. The delays are longer in case of high IWV and heavier precipitation than in the case of smaller IWV, which is consistent with our analysis as heavy precipitation is usually formed by deeper clouds [e.g., *Gagin et al.*, 1985; *Rosenfeld et al.*, 1990] and hence likely to fall from a higher average altitude.

We have implicitly assumed a Lagrangian perspective in our analysis, although the precipitating systems move with respect to the instruments. This means that we might not observe the actual mature stage of the systems, but we can still define a "mature" stage relative to the observation and not to the system (i.e., this is the most mature stage observed). The motion of the systems with respect to the instruments makes it difficult to untangle the effects of the in-cloud processes from advection. Additional measurements will be needed to deepen the analysis (see next section). The observed decrease of IWV can be interpreted as a consequence of the subsidence often associated with the decay of a precipitating system and/or the condensation/deposition occurring without compensation by moisture convergence. In case of a stationary system being advected over the measurement site, the observed evolution of IWV should be interpreted in terms of the system's spatial structure rather than its lifecycle. For instance, cold-frontal precipitation rainbands in midlatitude cyclones have a leading warm sector [*Houze*, 1993], which will have a higher IWV. However, the surface air temperature (not shown) does not show any sign of such cold-frontal systems predominating, as on average there is no significant temperature increase before the precipitation (but rather a decrease associated with the precipitation).

Like IWV, the MR increases before the start of the precipitation, but then increases even faster after the onset of precipitation and does not decrease significantly before precipitation ends. At the start of precipitation the increase in MR can be explained by both the evaporation of precipitation and the moisture flux convergence. The strength of the increase can be explained by the combination of these two effects and the absence of any compensating mechanism. Indeed, unlike at higher altitudes, at the surface there is no cloud formation and

hence no condensation sink. After the precipitation peak, MR stays constant. Although we could expect a divergence of the water vapor flux associated with the decay of the system (as well as being synoptically-induced), evaporation of falling precipitation and evapotranspiration from the surface can supply enough water vapor to maintain constant MR.

In the cases of high IWV, we observed higher precipitation likely to lead to a moister surface and hence larger evaporation for a longer time. This can explain the longer delay between the end of precipitation and the decrease in the MR observed in the HIWV cases (compared to the MIWV cases).

4.3. Perspectives

This study presents some results and hypotheses, as well as posing questions for future work. It could be interesting, for instance, to combine the data with meteorological analysis or model output and satellite observations to discriminate between different precipitation regimes. It could be then possible to determine the structure and likelihood of occurrence of different types of precipitating systems (e.g., frontal rainbands, mesoscale convective systems, local summertime convection, and orographic precipitation; cf. *Houze*, 1993) and then investigate the specific relationship between IWV and precipitation for each type of system. An extension of this study to other locations could also be interesting in order to identify any site-dependencies and to perform inter-comparisons using the numerous GPS data available worldwide [e.g., *Sguerso et al.*, 2015].

In order to further the understanding of the precipitation lifecycle, it would also be highly valuable to combine GPS measurement of IWV with MWR and polarimetric cloud radar measurements of cloud liquid water and cloud ice content. Such a network of combined continuous GPS and MWR measurements could then provide a 3-D reconstruction of water content in its three phases, although achieving the required high resolution would be challenging. Likewise, a more complete description of precipitation measurement could be complemented by the use of a network of pluviometer and high-resolution precipitation radar. Such a comprehensive study would allow the effects of advection to be separated from those of in-cloud processes and enable the importance of the different parameters in play to be determined, alongside the importance of changes from one phase of water to another. Finally, detailed water budgets and comparisons with cloud resolving models could lead to a better understanding of the underlying microphysical processes and pathways in various precipitating systems.

Acknowledgments

The GPS-derived tropospheric data (zenithal total delays (ZTDs)) calculated by the Institut national de l'information géographique et forestière (IGN) can be accessed via ftp from the Reseau GNSS Permanent (RGP): rgpdata.ign.fr, in the directories /pub/products/troposphere/hourly_1/YYYY/DDD (YYYY being the year and DDD the day of year). The ZTDs are in the hourly *sgn* files. The data used in this paper are for the station CLFD. The IWVs derived from these ZTD and the meteorological data can be accessed by contacting the corresponding author. The authors want to thank and acknowledge the LaMP/OPGC staff for the instrumentation operation and maintenance that made the data set available. The ZTD values used in this study have been produced and distributed by the IGN in the scope of the RGP. Special thanks go to Georgia Roesh and Romain Pages who provided support and valuable explanation about the processing strategy. The lead author would like to acknowledge Guy Delrieu (LTHE), Carole Legorgeu, and Wolfram Wobrock (LaMP/ Universite Blaise Pascal) for interesting discussions and comments. We also would like to acknowledge Bethan White (University of Oxford) for proofreading and commenting the manuscript. We also thank the two reviewers for their useful questions and comments.

References

Banacos, P. C., and D. M. Schultz (2005), The use of moisture flux convergence in forecasting convective initiation: Historical and operational perspectives, *Weather Forecasting*, *20*(3), 351–366, doi:10.1175/WAF858.1.

Bastin, S., C. Champollion, O. Bock, P. Drobinski, and F. Masson (2005), On the use of GPS tomography to investigate water vapor variability during a Mistral/sea breeze event in southeastern France, *Geophys. Res. Lett.*, *32*, L05808, doi:10.1029/2004GL021907.

Beard, K. V. (1976), Terminal velocity and shape of cloud and precipitation drops aloft, *J. Atmos. Sci.*, *33*(5), 851–864, doi:10.1175/1520-0469(1976)033<0851:TVASOC>2.0.CO;2.

Bevis, M., S. Businger, T. Herring, C. Rocken, R. Anthes, and R. Ware (1992), GPS meteorology: Remote sensing of atmospheric water vapor using the Global Positioning System, *J. Geophys. Res.*, *97*(D14), 15,787–15,801, doi:10.1029/92JD01517.

Bonafoni, S., A. Mazzoni, D. Cimini, M. Montopoli, N. Pierdicca, P. Basili, P. Ciotti, and G. Carlesimo (2013), Assessment of water vapor retrievals from a GPS receiver network, *GPS Solutions*, *17*, 475–484, doi:10.1007/s10291-012-0293-5.

Brenot, H., A. Walpersdorf, M. Reverdy, J. Van Baelen, V. Ducrocq, C. Champollion, F. Masson, E. Doerflinger, P. Collard, and P. Giroux (2014), A GPS network for tropospheric tomography in the framework of the Mediterranean hydrometeorological observatory Cévennes-Vivarais (southeastern France), *Atmos Meas Tech*, *7*(2), 553–578, doi:10.5194/amt-7-553-2014.

Champollion, C., F. Masson, J. V. Baelen, A. Walpersdorf, J. Chéry, and E. Doerflinger (2004), GPS monitoring of the tropospheric water vapor distribution and variation during the 9 September 2002 torrential precipitation episode in the Cévennes (southern France), *J. Geophys. Res.*, *109*, D24102, doi:10.1029/2004JD004897.

Champollion, C., C. Flamant, O. Bock, F. Masson, D. D. Turner, and T. Weckwerth (2009), Mesoscale GPS tomography applied to the 12 June 2002 convective initiation event of IHOP_2002, *Q. J. R. Meteorol. Soc.*, *135*(640), 645–662, doi:10.1002/qj.386.

Ciach, G. J. (2003), Local random errors in tipping-bucket rain gauge measurements, *J. Atmos. Oceanic Technol.*, *20*(5), 752–759, doi:10.1175/1520-0426(2003)20<752:LREITB>2.0.CO;2.

Davis, J. L., T. A. Herring, I. I. Shapiro, A. E. E. Rogers, and G. Elgered (1985), Geodesy by radio interferometry: Effects of atmospheric modeling errors on estimates of baseline length, *Radio Sci.*, *20*(6), 1593–1607, doi:10.1029/RS020i006p01593.

Ducrocq, V., D. Ricard, J.-P. Lafore, and F. Orain (2002), Storm-scale numerical rainfall prediction for five precipitating events over france: on the importance of the initial humidity field, *Weather Forecasting*, *17*(6), 1236–1256, doi:10.1175/1520-0434(2002)017<1236:SSNRPF>2.0.CO;2.

Emardson, T. R., and H. J. P. Derks (2000), On the relation between the wet delay and the integrated precipitable water vapour in the European atmosphere, *Meteorol. Appl.*, *7*(1), 61–68, doi:10.1017/S1350482700001377.

Gagin, A., D. Rosenfeld, and R. E. López (1985), The relationship between height and precipitation characteristics of summertime convective cells in South Florida, *J. Atmos. Sci.*, *42*(1), 84–94, doi:10.1175/1520-0469(1985)042<0084:TRBHAP>2.0.CO;2.

Holloway, C. E., and J. D. Neelin (2010), Temporal relations of column water vapor and tropical precipitation, *J. Atmos. Sci.*, *67*(4), 1091–1105, doi:10.1175/2009JAS3284.1.

Houze, R. A. (1993), *Cloud Dynamics*, *Int. Geophys. Ser.*, vol. 53, Acad. Press, San Diego, Calif.
Kalthoff, N., B. Adler, C. Barthlott, U. Corsmeier, S. Mobbs, S. Crewell, K. Träumner, C. Kottmeier, A. Wieser, and V. Smith (2009), The impact of convergence zones on the initiation of deep convection: A case study from COPS, *Atmos. Res.*, *93*, 680–694, doi:10.1016/j.atmosres.2009.02.010.
Kealy, J., J. Foster, and S. Businger (2012), GPS meteorology: An investigation of ocean-based precipitable water estimates, *J. Geophys. Res.*, *117*, D17303, doi:10.1029/2011JD017422.
Labbouz, L., J. Van Baelen, F. Tridon, M. Reverdy, M. Hagen, M. Bender, G. Dick, T. Gorgas, and C. Planche (2013), Precipitation on the lee side of the Vosges Mountains: Multi-instrumental study of one case from the COPS campaign, *Meteorol. Z.*, *22*(4), 413–432, doi:10.1127/0941-2948/2013/0413.
Manning, T., K. Zhang, W. Rohm, S. L. Choy, and F. Hurter (2012), Detecting severe weather using GPS tomography: An Australian case study, *J. Global Positioning Syst.*, *11*(1), 58–70, doi:10.5081/jgps.11.1.58.
Mazany, R. A., S. Businger, S. I. Gutman, and W. Roeder (2002), A lightning prediction index that utilizes GPS integrated precipitable water vapor, *Weather Forecasting*, *17*(5), 1034–1047, doi:10.1175/1520-0434(2002)017<1034:ALPITU>2.0.CO;2.
Planche, C., W. Wobrock, A. I. Flossmann, F. Tridon, L. Labbouz, and J. Van Baelen (2013), Small scale topography influence on the formation of three convective systems observed during COPS over the Vosges Mountains, *Meteorol. Z.*, *22*(4), 395–411, doi:10.1127/0941-2948/2013/0402.
Rosenfeld, D., D. Atlas, and D. A. Short (1990), The estimation of convective rainfall by area integrals: 2. The Height-Area Rainfall Threshold (HART) method, *J. Geophys. Res.*, *95*(D3), 2161–2176, doi:10.1029/JD095iD03p02161.
Saastamoinen, J. (1972a), Contributions to the theory of atmospheric refraction, *Bull. Géod.*, *105*, 279–298, doi:10.1007/BF02521844.
Saastamoinen, J. (1972b), Introduction to practical computation of astronomical refraction, *Bull. Géod.*, *106*, 383–397, doi:10.1007/BF02522047.
Sato, T., and F. Kimura (2005), Diurnal cycle of convective instability around the central mountains in Japan during the warm season, *J. Atmos. Sci.*, *62*(5), 1626–1636, doi:10.1175/JAS3423.1.
Sguerso, D., L. Labbouz, and A. Walpersdorf (2015), 14 years of GPS tropospheric delays in the French–Italian border region: Comparisons and first application in a case study, *Appl. Geomat.*, *1–13*, doi:10.1007/s12518-015-0158-z.
Sherwood, S. C., R. Roca, T. M. Weckwerth, and N. G. Andronova (2010), Tropospheric water vapor, convection, and climate, *Rev. Geophys.*, *48*, RG2001, doi:10.1029/2009RG000301.
Solheim, F. S., J. Vivekanandan, R. H. Ware, and C. Rocken (1999), Propagation delays induced in GPS signals by dry air, water vapor, hydrometeors, and other particulates, *J. Geophys. Res.*, *104*(D8), 9663–9670, doi:10.1029/1999JD900095.
Tregoning, P., R. Boers, D. O'Brien, and M. Hendy (1998), Accuracy of absolute precipitable water vapor estimates from GPS observations, *J. Geophys. Res.*, *103*(D22), 28,701–28,710, doi:10.1029/98JD02516.
Trenberth, K. E., A. Dai, R. M. Rasmussen, and D. B. Parsons (2003), The changing character of precipitation, *Bull. Am. Meteorol. Soc.*, *84*(9), 1205–1218, doi:10.1175/BAMS-84-9-1205.
Van Baelen, J., and G. Penide (2009), Study of water vapor vertical variability and possible cloud formation with a small network of GPS stations, *Geophys. Res. Lett.*, *36*, L02804, doi:10.1029/2008GL036148.
Van Baelen, J., J.-P. Aubagnac, and A. Dabas (2005), Comparison of near–real time estimates of integrated water vapor derived with GPS, radiosondes, and microwave radiometer, *J. Atmos. Oceanic Technol.*, *22*, 201–210, doi:10.1175/JTECH-1697.1.
Van Baelen, J., M. Reverdy, F. Tridon, L. Labbouz, G. Dick, M. Bender, and M. Hagen (2011), On the relationship between water vapour field evolution and the life cycle of precipitation systems, *Q. J. R. Meteorol. Soc.*, *137*(S1), 204–223, doi:10.1002/qj.785.
Weckwerth, T. M., L. J. Bennett, L. Jay Miller, J. van Baelen, P. Di Girolamo, A. M. Blyth, and T. J. Hertneky (2014), An observational and modeling study of the processes leading to deep, moist convection in complex terrain, *Mon. Weather Rev.*, *142*(8), 2687–2708, doi:10.1175/MWR-D-13-00216.1.